JOURNAL OF GEOPHYSICAL RESEARCH, VOL. 91, NO. C6, PAGES 7573-7585, JUNE 15, 1986

Synoptic Gulf Stream Velocity Profiles Through Simultaneous Inversion of Hydrographic and Acoustic Doppler Data

T. M. JOYCE

Woods Hole Oceanographic Institution, Woods Hole, Massachusetts

C. WUNSCH

Department of Earth, Atmospheric and Planetary Sciences, Massachusetts Institute of Technology, Cambridge

S. D. PIERCE

Joint Program in Oceanography, Massachusetts Institute of Technology/Woods Hole Oceanographic Institution Woods Hole, Massachusetts

Data from a shipborne acoustic profiling device have been combined with conductivity, temperature, depth/O_2 sections across the Gulf Stream to form estimates of the absolute flow fields. The procedure for the combination was a form of inverse method. The results suggest that at the time of the observations (June 1982) the net Gulf Stream transport off Hatteras was 107 ± 11 Sv and that across a section near 72.5°W it had increased to 125 ± 6 Sv (subject to further uncertainty from the definition of the stream). The transport of the deep western boundary current was 9 ± 3 Sv. These and other transport estimates are plausibly close to previous calculations, but we do not claim that they represent the temporal mean. For comparison purposes we have done an inversion using the hydrographic/O_2 data alone as in previously published results and obtained qualitative agreement with the combined inversion. Inversion of the acoustic measurements alone, when corrected for instrument biases, leaves unacceptably large mass transport residuals in the deep water. Our conclusion is that the inversion of the combined data sets produces results much improved over those from using either acoustic or hydrographic/chemical constraints in isolation. The procedures are close analogues to those which can be used with satellite altimeters and are a procedure for obtaining very accurate geoid slope measurements.

1. INTRODUCTION

During a time series study of Gulf Stream warm-core ring 82B, data were collected on two transects which extended from the outer edge of the continental shelf across the slope water and Gulf Stream into the Sargasso Sea. The purpose of these sections was to define the circulation and water mass distribution in the "undisturbed" water on either side of the ring [*Olson et al.*, 1985, Figure 1*d*]. During a 3.5-day period from June 26 to 29, 1982, the R/V *Endeavor* was used to obtain a series of conductivity, temperature, depth (CTD)/O_2 stations across the Gulf Stream–slope water as shown in Figure 1. Simultaneous measurements were made of the absolute near-surface velocity by use of an underway acoustic profiling device [*Joyce et al.*, 1982].

Previous estimates of near-synoptic absolute velocities near the Gulf Stream have been based upon hydrographic data plus sparse arrays of neutrally buoyant floats [e.g., *Volkmann*, 1962] or discrete current meter or shipborne transport measurements [e.g., *Richardson*, 1977; *Halkin and Rossby*, 1985]. The dense spatial coverage of the acoustic profiling system suggests that much of the spatial aliasing error that is unavoidable with sparse sampling might be eliminated here, and we may be able to obtain much more certain estimates of water mass flux rates in this region. In addition, these measurements present an interesting opportunity to do a number of things: to better understand the accuracy and precision of the acoustic profiler, to do a combined inversion of the hydrography with the acoustic data so as to make a best estimate of the absolute velocity field, and to make a direct comparison between the velocity field determined from a geostrophic inversion of the type described by *Wunsch* [1978] with an independent estimate.

Another intriguing feature of this data set is that the acoustic velocities provide an analogue for altimetrically derived data sets, which are hoped for in the next several years. (The combination of altimetry with hydrography was studied by *Wunsch and Gaposchkin* [1980] and *Roemmich and Wunsch* [1982], but no actual combined data have been available for use). *Pollard* [1983] successfully compared a hydrographic inversion with simultaneous current meter measurements, but to our knowledge no one has previously had a data set resembling the present one.

The structure of this paper is as follows. We will first pursue our primary aim of making a best estimate of the absolute flow field, and we will discuss the resulting circulation. Having done that, we will take our estimation (inverse) procedure apart in order to compare estimates of the velocity field in which the acoustical constraints are withheld and with those in which the conservation constraints are withheld and in order to compare both with estimates from the combined form.

2. DESCRIPTION OF DATA

On *Endeavor* cruise EN86, two sections were occupied with CTD/O_2 casts to the bottom with a nominal station spacing

Paper number 6C0147
0148-0227/86/006C-0147$05.00

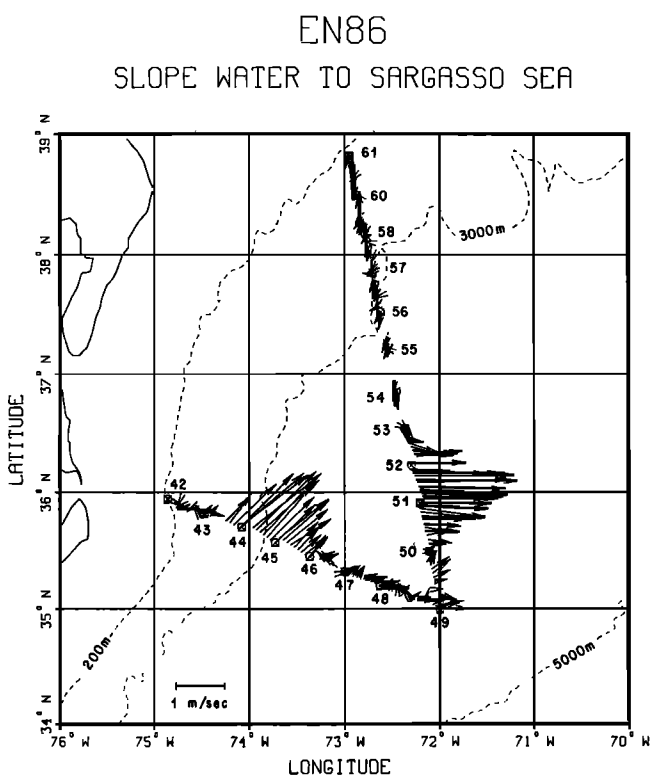

Fig. 1. Positions of the CTD/O_2 stations from *Endeavor* cruise 86 used in this study. Station numbers and the 60-m horizontal velocity as measured by the acoustic profiling device are shown. The two sections are referred to as "south" and "north".

of 37 km. The CTD data were collected with an NBIS unit and were processed by the Woods Hole Oceanographic Institution (WHOI) CTD group. The near-surface velocity field was sampled while underway and on station with a 300-KHz Ametek-Straza transducer. The velocities used in this study were obtained by vector averaging 10-min blocks of Doppler data and combining this average with a LORAN-C-derived ship velocity over the earth. Noise in the latter introduces a 10-cm/s uncertainty in the absolute currents for each 10-min interval. Because the velocities were further averaged, producing a single velocity estimate between CTD stations, this random error is reduced to approximately 3 cm/s. We have chosen to use the currents at 60-m depth as a compromise between the need to measure below the surface mixed layer yet avoid interference with the bottom, which is as shallow as 90 m at the southwest vertex of the triangle of stations (CTD station 42, Figure 1).

We will refer to the section consisting of stations 42–49 as the "south" section and to the section consisting of stations 49–61 as the "north" section as shown in Figures 2 and 3, respectively. The variables plotted are potential temperature, salinity, oxygen, and potential density referred to the surface. Over the strongly sloping isolines of all variables, the core of the eastward flowing Gulf Stream is defined on both sections by its warm surface temperatures and the subsurface salinity maximum (greater than 36.6) in the upper 200 m. In the deep water, the signature of the deep western boundary current (DWBC) can be found in the oxygen distribution, specifically the begions of >6.1 mL/L at depths of 3000 m. The small bubble of high oxygen at stations 43 and 44 over the continental slope on the south section (also present in a section of *Worthington and Kawai* [1972]) is probably a remnant of Labrador Sea water. It will be shown below that these deep layers of relatively high oxygen are moving in opposition to the Gulf Stream.

The velocity field will be estimated in this paper by three methods: direct use of the 18 current measurements to define a reference level, an inverse method (not using velocity measurements), and a combined inversion using hydrographic, O_2, and velocity data. All three methods assume geostrophy and mass balance, and they assume that mass flow from the outer shelf into the slope water is negligible. *Beardsley and Boicourt* [1981] estimate the volume transport over the continental shelf to be 0.2×10^6 m^3/s. In view of the large transports of water over the slope and in the Gulf Stream, the potential error in the mass balance assumption should be small. Figure 1 suggests that the Gulf Stream path curves; hence centripetal accelerations may be important. If the radius of curvature is taken to be 200 km, then in the upper waters of the Gulf Stream the "cyclostrophic" term may be as much as 0.08 of the Coriolis term in the cross-stream momentum balance. Were the Doppler system to penetrate deeper into the water column than about 100 m, we would be able to investigate the degree to which the Gulf Stream thermal wind balance holds. For now, we will proceed assuming geostrophy.

The average velocity at 60 m between station pairs was used as a reference for geostrophic calculations throughout the water column. Once this was done, the total transport for each section was determined. Initially, the volume transport across the south section was 42×10^6 m^3/s greater than that across the north section. The two transports could be made to balance by subtracting a constant offset of 1.9 cm/s from velocities on the south section and adding the same value to the velocities on the north section. We believe this value to be due to a systematic bias in the Doppler velocities, best understood as follows.

If one decomposes Doppler currents into components parallel and perpendicular to a vector defined by the ship's motion over the earth, then an error, $\delta\theta$, in the transducer alignment and ship gyro compass, for a ship speed U, will produce an apparent athwartship velocity of $U \sin \delta\theta$.

Both $\delta\theta$ and U must be estimated. Calibration runs to determine θ are limited by the ability to estimate ship velocity over the earth. This procedure is discussed by *Joyce et al.* [1982]. The Northstar 6000 LORAN receiver employed has an observed noise level (J. McCullough, personal communication, 1985) of 0.1 μs or ± 30 m. Ship velocities calculated by differencing two positions separated in time by an amount Δt will have an uncertainty of $\pm 30\sqrt{2}/\Delta t$. For a 10-min measurement period this uncertainty is ± 7 cm/s in each horizontal velocity component, corresponding to the speed uncertainty of 10 cm/s noted above. Least squares fits used in the present analysis produce errors consistent with these estimates. An error in ship speed, δU, will for small θ produce an uncertainty $\delta\theta$ equal to $\delta U/U$. For a ship speed $U = 5$ m/s, an error in ship velocity of $\delta U = 2.6$ cm/s is equivalent to an angular uncertainty $\delta\theta = 0.3°$. These numbers reflect the a priori levels of confidence in the Doppler data. Note that this angular "offset" error will be systematically to the right or left of the ship track. Because the cruise track (Figure 1) crossed the Gulf Stream in opposite directions, the bias in athwartship velocities will be approximately constant and of opposite signs in the two sides of the triangle.

The 1.9-cm/s correction applied to conserve mass is well within the bounds to be expected. The resulting corrected ve-

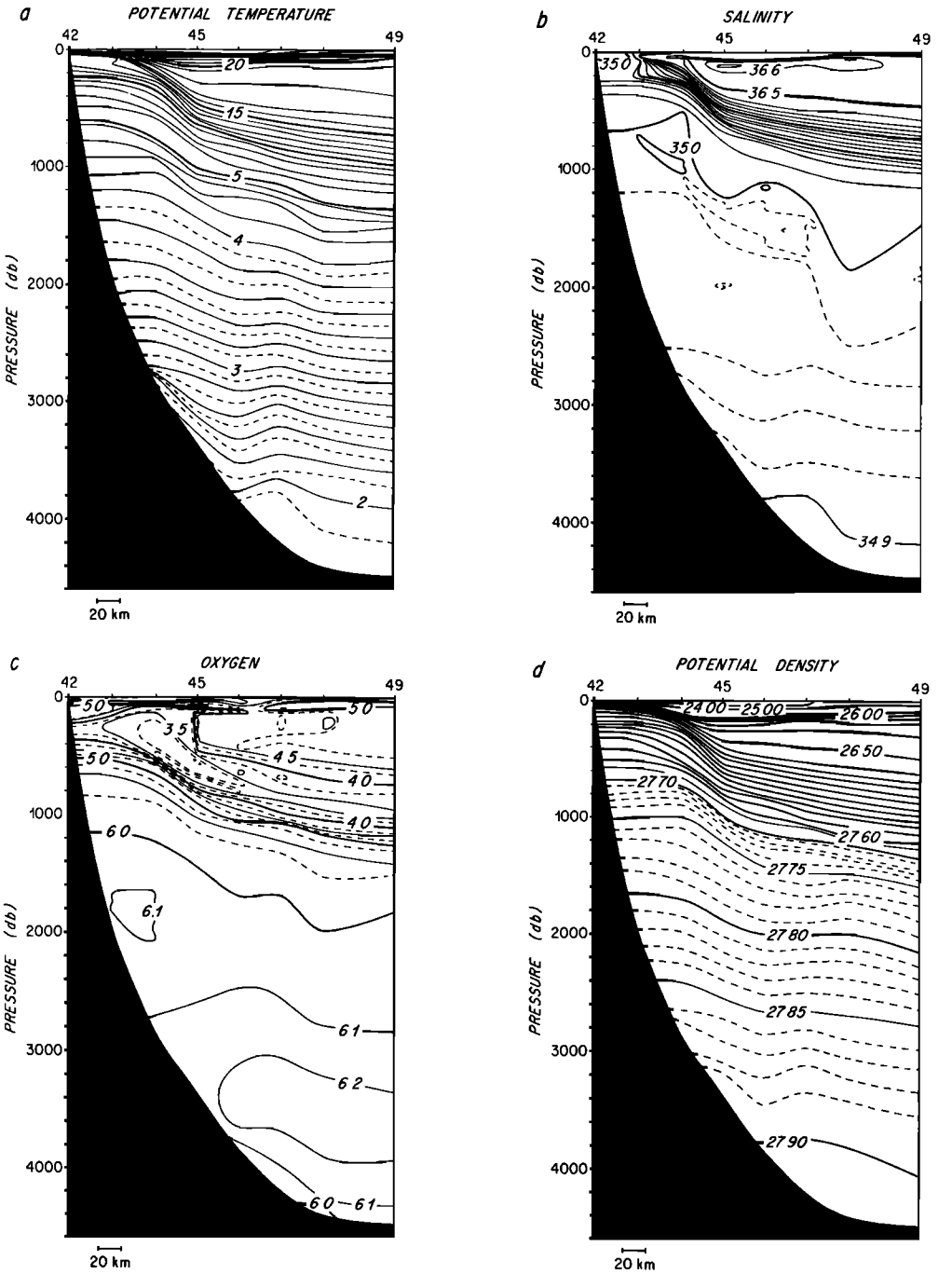

Fig. 2. Property distributions (potential temperature, salinity, O_2, and σ_θ) for the south section.

locity sections are shown in Figure 4. In the south section the Gulf Stream extends to the bottom with a weak counterflow over the continental slope and a stronger southward flow (DWBC) in the deep water under the Gulf Stream. The currents in the slope water (north section) are opposite to the Gulf Stream and extend to the bottom, with a suggestion of a near-surface maximum exceeding 10 cm/s similar to that described by *Webster* [1969] and *Hogg* [1983]. Deep currents on the north section are weaker than those to the south, with deep flow to the southwest except under the Gulf Stream. The regions of high oxygen in the deep water on both sections generally have velocities opposite to the Gulf Stream.

Although Figure 4 might be regarded as a reasonable estimate of the absolute flow in the sections, examination of the "pure acoustic" transports involved shows that large imbalances exist in the deeper water masses. Table 1 lists isopycnals used to subdivide the water column into 13 layers. We find, for example, that in layers 7–12, approximately 7.8 Sv more fluid enters the volume than leaves it. We believe these imbalances are too large to be physically acceptable and that by demanding their removal we can learn more about the structure of the true flow field. A systematic procedure for removing the imbalances is applied in the next section.

3. Estimates of the Absolute Ocean Velocity Field

We seek a best estimate of the absolute flow field in the sections of Figure 1; the estimate will be required to satisfy

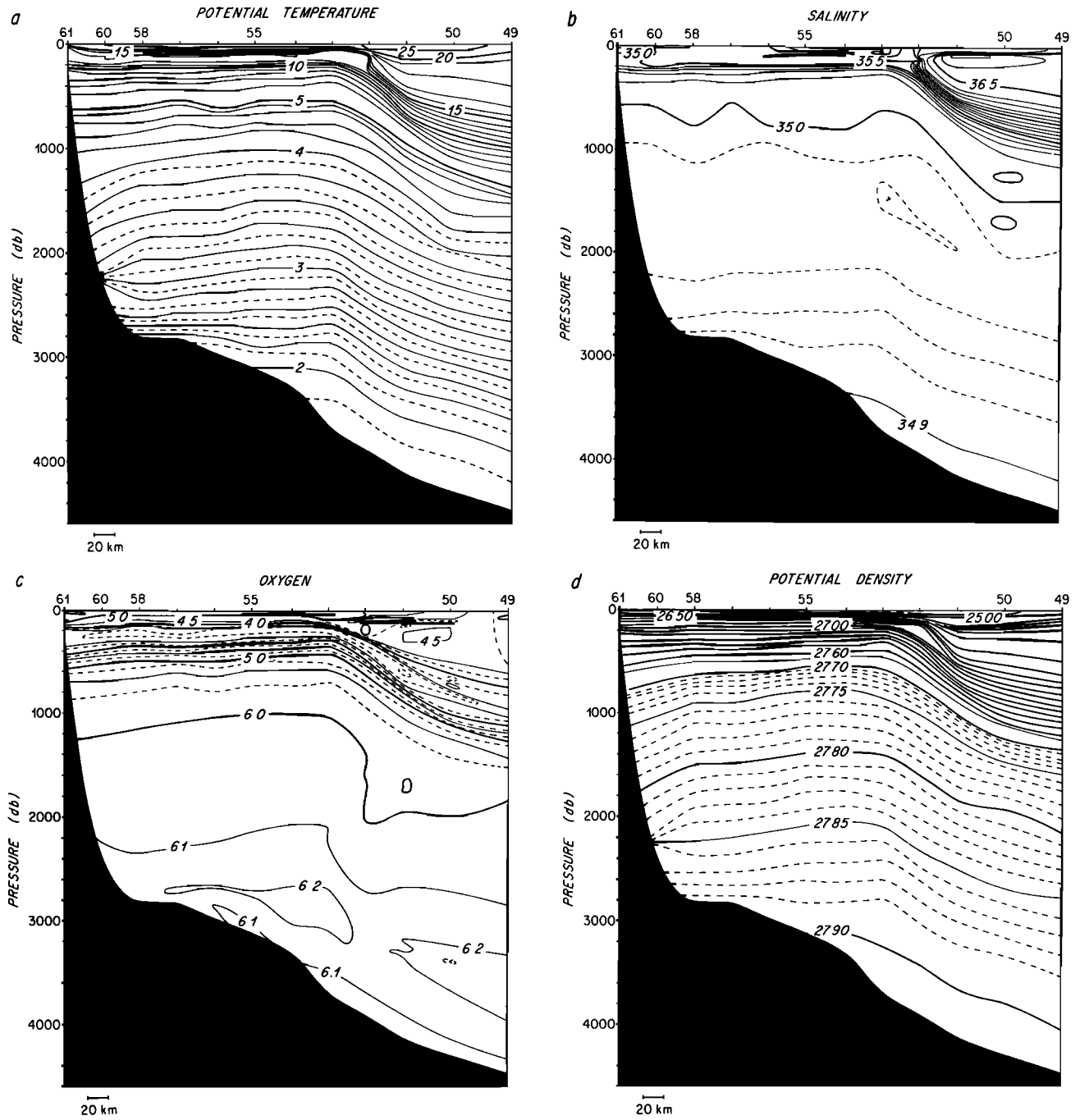

Fig. 3. Same as Figure 2, but for the north section.

several plausible restrictions: the velocity should be consistent with the acoustic data within the error bars of the measurement, and within estimated errors, the resulting flow should conserve (1) total mass, (2) total salt, (3) mass and salt within and between intermediate layers, and (4) oxygen within and between intermediate layers not near the surface. These requirements appear minimal for any flow field that is to be regarded as physically realistic.

To begin, we choose a deep reference level at 2000 dbar. Some comment about this initial choice is required. The hydrography plus a reference level (which could be more complex than a constant pressure) represents an initial conceptual model of the ocean. It should be chosen so as to encompass everything we think we know with any confidence about the oceanic behavior in the absence of any further information. New information will usually require modifications to this initial model. But if we are sensible, we should arrange things so that if the noise levels in the new information grow arbitrarily large, our estimates of the oceanic flow reduce back to the initial state.

Let the unknown reference level velocity in station pair j be denoted b_j. If we integrate the profiler-determined 60-m velocity downward to the 2000-dbar reference level via the thermal wind relation, we obtain a set of equations for the true reference level velocity of the form

$$b_j = \alpha_j \pm \varepsilon_j \qquad j = 1, 18 \tag{1}$$

for each station pair, where α_j is the acoustic reference level velocity. As was already stated, the errors ε_j in (1) are estimated to have a random component of about 3 cm/s rms, a

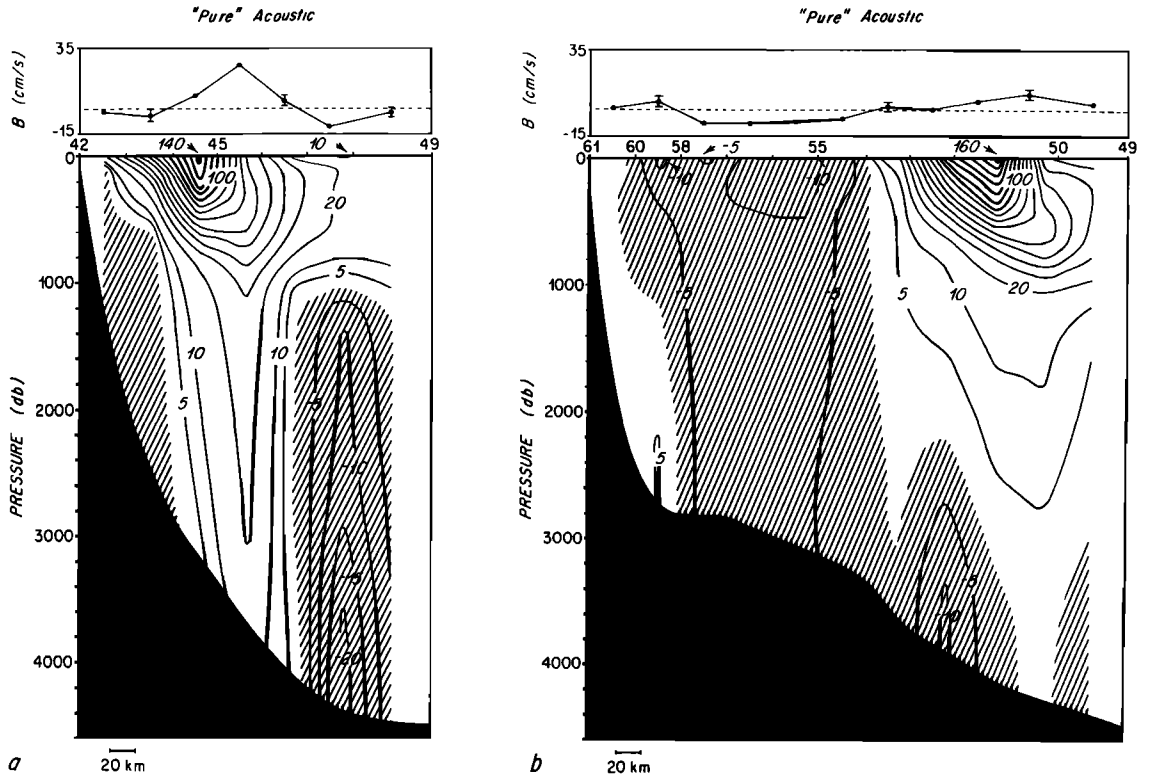

Fig. 4. Velocity field as determined from thermal wind and 60-m acoustic velocity corrected only for an average bias of 1.9 cm/s in order to conserve mass overall. (*a*) South section. (*b*) North section.

systematic component (the bias) of about the same magnitude, plus an additional error due to inaccuracies in the thermal wind computation. These latter errors are assumed to be small in comparison with the other two. The sign of the bias is unknown a priori.

The further constraints on the flow are of the same form as those written by *Wunsch* [1978] and *Wunsch et al.* [1983] and are as follows. The ocean was divided into 13 layers listed in Table 1; these layers were chosen to resolve in the vertical all of the major water mass structures of the region. The total flow field is composed of two parts: the horizontal velocity $v_j + b_j$, where v_j is the thermal wind component in each station pair j and b_j is the reference level velocity there, and the cross-isopycnal velocity w_i^* across density interface i lying between layers i and $i + 1$ [see *Wunsch et al.*, 1983]. There are $j = 1$, 18 station pairs and $i = 1$, 12 interface velocities in the present geometry.

The total velocity field is required to satisfy a number of requirements. We demand conservation of mass and salt in the entire volume, conservation of both in each of the layers, and oxygen conservation in each layer below the surface one. Each of these conservation demands is a linear relationship between the geostrophically computed inflow and outflow, the transfers across upper and lower bounding isopycnals, and the areas of the bounding surfaces. Because the observations are imperfect and because the purely geostrophic model is not complete, none of the conservation conditions is to be satisfied perfectly but should leave an error which we will discuss below.

Any of the conservation requirements described can be written as

$$\sum_{j=1}^{18} a_{pj}(b_j + v_j) + a_{pi}'w_i^* + a_{p,i-1}'w_{i-1}^* \simeq 0 \qquad (2)$$

where the label p refers to the pth requirement and the coefficients are the appropriate property concentration times the corresponding boundary area times a factor of ± 1 to represent the sign of the unit normal of the volume. Write the combined set of unknowns b_j, w_i as a column vector

$$\mathbf{q} = \begin{bmatrix} \mathbf{b} \\ \cdots \\ \mathbf{w} \end{bmatrix}$$

Then the complete set of near-conservation requirements can be written in the form

$$\mathbf{Aq} = -\mathbf{d} \qquad (3)$$

$\mathbf{A}$ is made up of the elements a_{pj}, a_{pi}'; the elements of $\mathbf{d}$ comprise the initial imbalances of mass/salt/O_2 before any inversion is carried out and involve terms of form $\sum a_{pj}v_j$. We have already noted that if the initial reference level velocities are put equal to the acoustic measurements, then total mass is initially out of balance by about 40 Sv.

It is not altogether clear how precisely (3) should be satisfied (i.e., what is the expected error in $\mathbf{d}$?). There are many sources of error: (1) the hydrographic stations were obtained over 3.5 days; *Halkin and Rossby* [1985] found shifts in transport of the Gulf Stream of 10 Sv over 7 days, so that there is some degree of aliasing in the data set; (2) there could be temporary storage terms leading to missing time dependences in equation 3; (3) we have ignored cyclostrophic effects in the Gulf Stream; and (4) there could be a variety of measurement errors. Without being very firm about it, we estimated that total mass should be conserved to about 0.1 Sv, and to about 0.3 Sv in any individual layer, with equivalent values for salt and oxygen.

The 18 equations of (1) can be simply appended to the mass,

TABLE 1. Isopycnals Used to Define Layers for Budgeting Purposes and Mass Transports in Each Layer for Different Flow Solutions

		Combined Rank 25		Combined Rank 30		Pure Acoustic		Pure Hydrographic	
Layer	σ_θ	South	North	South	North	South	North	South	North
1	surface–24.00	2.1	1.8	2.1	1.8	2.1	1.8	1.9	1.6
2	24.00–25.00	4.9	5.7	4.7	5.6	4.6	5.5	4.7	5.1
3	25.00–26.50	31.6	29.5	29.5	28.2	28.3	28.4	26.7	25.5
4	26.50–27.00	28.2	29.3	26.2	28.2	25.1	28.1	24.4	25.3
5	27.00–27.30	11.5	11.2	10.4	10.5	10.0	10.1	9.8	9.4
6	27.30–27.50	6.1	7.6	5.4	7.2	5.0	6.8	5.3	5.7
7	27.50–27.70	6.9	6.7	5.5	5.4	4.9	4.5	4.0	4.1
8	27.70–27.76	6.7	5.9	4.7	4.0	3.8	2.4	2.8	2.5
9	27.76–27.80	7.9	7.0	5.0	4.0	3.7	1.9	2.7	2.2
10	27.80–27.85	7.6	8.7	3.9	3.8	2.1	0.7	0.9	1.4
11	27.85–27.88	4.1	4.2	1.7	0.4	0.3	−1.8	−0.3	−0.5
12	27.88–27.90	2.1	1.9	−1.9	−3.4	−4.3	−5.0	−8.5	−8.6
13	27.90–bottom	−1.1	−0.9	−2.8	−1.0	−3.5	−1.5	−2.6	−2.7
Total		119	119	94.5	94.6	82.2	82.1	71.8	71.1

The sign convention is that a positive mass flux is to the north and east. The values represent the total integrated along the section. Units are 10^9 kg/s.

salt, and oxygen constraints of (3) to generate a combined set:

$$\mathbf{A'q = d'} \quad \mathbf{A'} = \begin{bmatrix} \mathbf{I}_{18} & \vdots & \mathbf{O} \\ \cdots & \cdots & \cdots \\ & \mathbf{A} & \end{bmatrix} \quad \mathbf{d'} = \begin{bmatrix} \alpha \\ \cdots \\ -\mathbf{d} \end{bmatrix} \tag{4}$$

$\mathbf{I}_{18}$ is the 18 × 18 identity matrix, and $\mathbf{O}$ is the 18 × 12 null matrix.

For each equation in the resulting combined set, a weighting factor was introduced so that the equation became nondimensional and had a weight inversely proportional to the estimated error in that equation. That is, the equations were multiplied by a numerical factor so that all scaled equations had unit expected error variance. This weighting is done as part of all conventional least squares schemes. A column weighting was also done so as to provide maximum numerical stability and to reflect our a priori estimate (described below) of the relative magnitudes of w_i* and b_i. It is not difficult to show that column weighting has no effect on the solution if the system is in fact overdetermined. Both forms of weighting are described in detail by *Lawson and Hanson* [1974], *Wiggins* [1972] and *Wunsch et al.* [1983]. From here on, $\mathbf{A'}$, $\mathbf{d'}$ and $\mathbf{q}$ denote the appropriate nondimensional scaled forms, but reference to $\mathbf{b}$ and $\mathbf{w}$* always is to the dimensional, unweighted ones.

The system (4) consists of 68 equations in the 18 unknown b_j plus 12 unknown w_i*. One may regard the values of the errors in each equation as an additional 68 unknowns if desired. As always, one needs to determine whether the rank of the system (4) is actually equal to 30, in which case all the unknowns are fully determined and we have a conventional regression problem, or whether it is rank deficient, leaving us with an inverse problem (as was discussed, for example, by *Wunsch* [1985], the distinction between these two types of problem is more apparent that real). As one example of the methods used here (and elsewhere), we show a plot in Figure 5 of the so-called Levenburg-Marquardt analysis (discussed by *Lawson and Hanson* [1974]), which displays the magnitude of the solution $\mathbf{q}$ against that of the residuals left in (4) from the solution. In regression theory the break in the curve where the solution magnitude increases rapidly with little or no reduction in residuals is interpreted as strong evidence that the best solution is the one (indicated by the arrow in the figure) having least variance for the same residuals. In the present problem the later, rapid drop in residuals for considerably increased solution magnitudes means that there is an alternative solution which we also need to study.

The solution procedure we chose to use was the singular value decomposition discussed by *Wunsch* [1978]; with this method not only is it easy to control the solution magnitude as a function of problem residual, but we also obtain a complete description of the problem structure. (The Levenburg-Marquardt solution procedure is equivalent and has the advantage of computational savings, but it has the disadvantage of providing less information about what is going on.) The solution magnitude indicated in Figure 5 corresponds to choosing a system rank k in the singular value decomposition of about $k = 25$. The minimum residual corresponds to the full rank $k = 30$.

At rank 25 the b_j are nearly fully determined (Figure 6), but the w_i* are only partially determined, as is shown in Figure 7*a*.

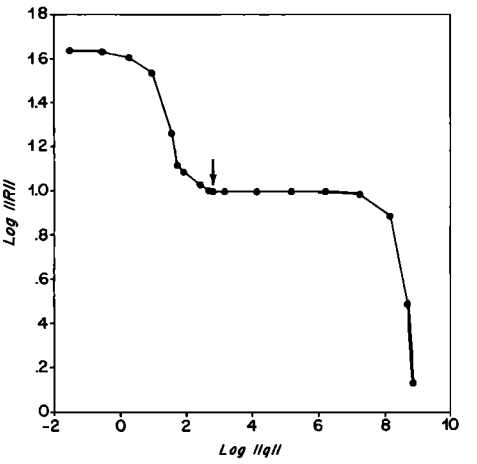

Fig. 5. Levenburg-Marquardt diagram showing reduction in constraint residuals as a function of solution magnitude and used to determine approximate system rank. The solution magnitude is indicated as being near the base of the initial drop-off, as denoted by the arrow, or alternatively, near the final, minimum, residual level.

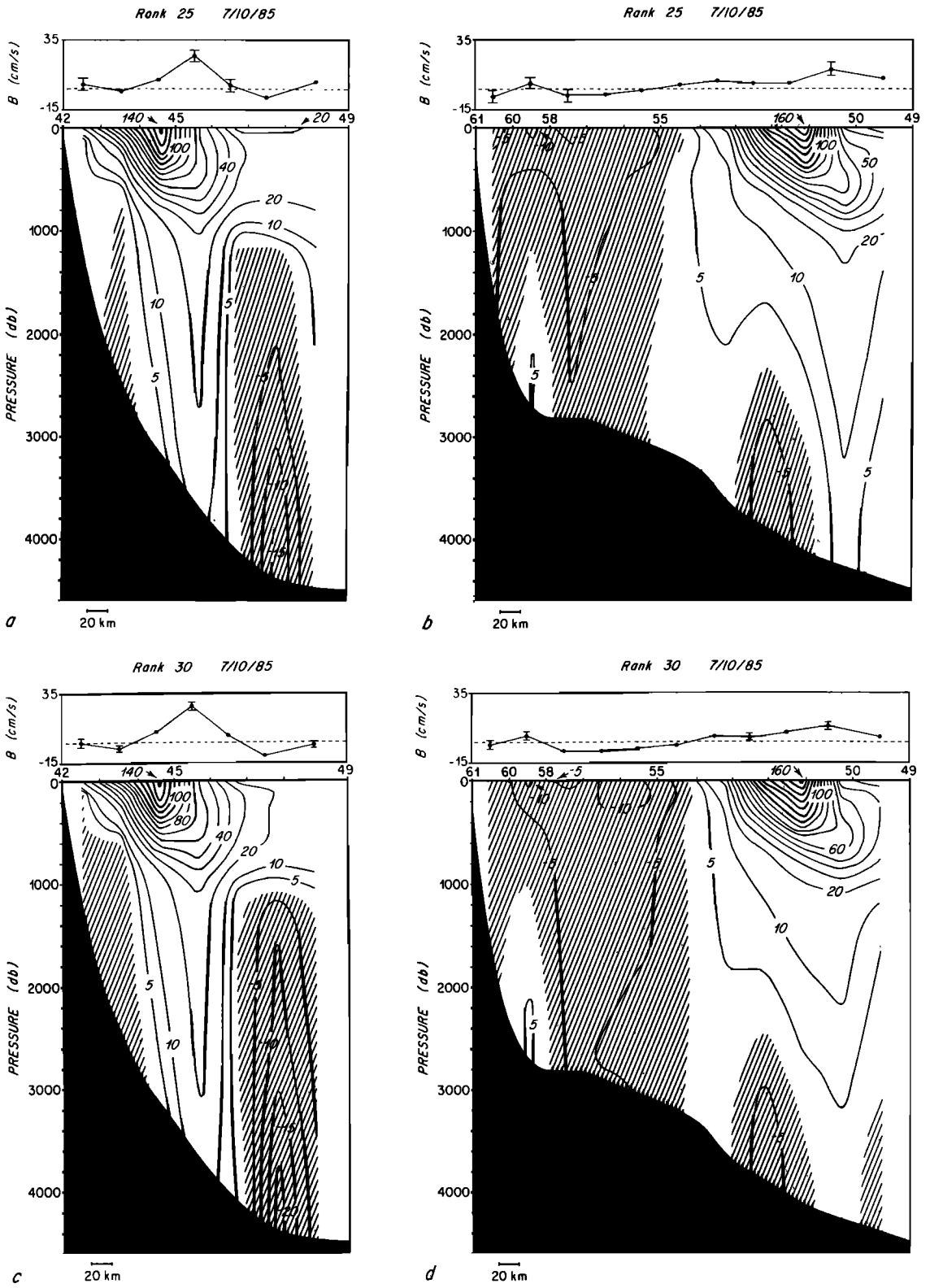

Fig. 6. Velocity sections for (*a*) rank 25 south, (*b*) rank 25 north, (*c*) rank 30 south, and (*d*) rank 30 north choices of combined inversion. We have some small preference for the rank 30 choice, but cannot really distinguish between them. Reference level velocities are shown at the top of each figure with an error bar which includes both the effects of noise and, for rank 25, the failure to resolve (for rank 30, all variables are formally fully resolved).

Our estimates of the absolute velocity sections are shown in Figures 6*a* and 6*b*.

There are residuals in all of the equations including the profiler subset. Figure 8 displays the difference between the acoustic profiler estimate of the reference level velocity and that determined from both the rank 25 and 30 inversions. The systematic offsets at rank 25 lead us to new estimates of the bias as 0.7 ± 3.8 and 4.3 ± 3.9 for the southern and northern

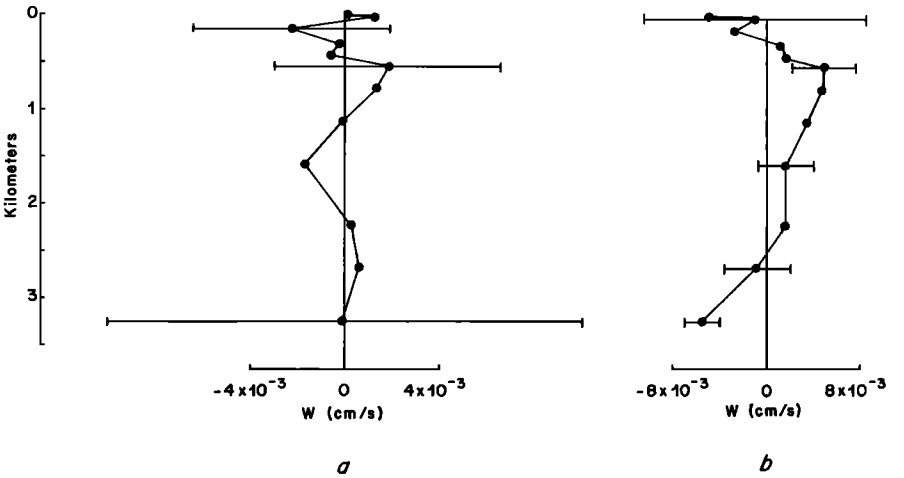

Fig. 7. Vertical mass transfers for (*a*) rank 25 and (*b*) rank 30 solutions with appropriate error bars. In the rank 25 case, error is dominated by the failure to resolve. In the rank 30 case it is wholly due to observational noise.

lines, respectively. When the bias is removed, the rms residuals of the acoustic velocity constraint equations (4) are ± 3.8 cm/s, reasonably consistent with our a priori estimate of 3-cm/s random noise in these measurements (there is a suggestion that we may have given slightly too little weight to the acoustic velocity constraints relative to the mass/salt/O_2 constraints).

The absolute velocity sections are shown in Figures 6*a* and 6*b*, with the actual reference level velocity determined from the inversion shown at the top, with error bars. The error bars have two contributors: (1) that due to the noise in the data and (2) that due to the failure to resolve all the energy lying in **b**, **w**. Estimating this latter error requires an a priori estimate of the magnitudes of **b**, **w***, something which is exceedingly elusive at the present state of our knowledge. But to give a rough idea of the error, the a priori variance in b_j was chosen to be that measured acoustically, i.e., α_j, and

$$\langle w_i^{*2} \rangle \cong (10^{-3} \text{ cm/s})^2$$

At rank 25, only 25 pieces of information about the 30 unknowns have been extracted from the data. Examination of the diagonal elements of the solution resolution matrix at rank 25 shows that all 18 of the reference level velocities have been nearly fully determined (diagonal element about 0.999) but the resolution of the w_i^* ranges from about 0.8 at the third interface downward to about 0.04 (between the bottom two layers). Figure 7*a* displays the w_i^* computed for this solution along with the appropriate error bars. (The error bar for the b_i is dominated by the data noise, as the values are almost fully resolved. If the variance $\langle b_i^2 \rangle \approx 900$ (cm/s)^2, then a resolution of 0.999 leaves a variance of $(1 - 0.999) * 900$ undetermined, or about 1 cm/s rms.)

In Figure 7*a*, generally speaking, the w_i^* are indistinguishable from 0. The question we raise is whether any more information about them can be extracted from the system. This question is equivalent to asking whether we have really used up all the information available in our observations. As part of any inverse procedure, one must examine the residuals in the original constraint equations which result from the model parameter determination. Figure 9 displays the mass balance residuals for our rank 25 solution. If the information has been exhausted, these residuals should be purely random (i.e., structureless white noise). In the present case, they are somewhat large and clearly structured, suggesting that there is more to be gained from the system. We have already noted a suspicion that the mass/salt/O_2 equations were given too much weight relative to the acoustic velocity equations, i.e., that the acoustic error may be less than 3 cm/s, which would account for a choice of rank which is too small. On the other hand, if we carry the rank to a maximum possible value of 30, then all parameters are fully determined (the system is then equivalent to a conventional overdetermined least squares problem), including the w_i^*. The solution for w_i^* resulting from a rank 30 choice is shown in Figure 7*b*; the difference between the acoustically determined and rank 30 reference velocities is shown in Figure 8, and the equation residuals are shown in Figure 9*b*. The error bars shown for w_i^* are now wholly due owing to data noise; we can see that an "upwelling" in the thermocline and a "downwelling" near bottom appear to be statistically significant in this new solution. Systematic offset, between acoustic and reference level velocities (Figure 8) are -1.2 ± 0.95 and 3.2 ± 1.5 cm/s for the south and north sections, respectively, at rank 30.

The mass transport residuals (Figure 9*b*) have been reduced in magnitude and are less structured. There is a hint that there is yet more information remaining. This result is a suggestion that a more complex model is required to fully explain the data. Such a model might, for example, encompass a more sophisticated from of cross-isopycnal mixing, permitting different rates for mass, salt, and oxygen. It is also possible that the remaining structure owes its origin to mass storage terms which are a function of depth. We conclude, however, that further pursuit of model complexity is not warranted with the present data set.

The final best estimates of the mass fluxes layer by layer are tabulated in Table 1. Figures 10 and 11 show the total transports and bottom water transports in each station pair for the two sections, as well as the sum accumulated from the northern end of each line. These results will be described more fully below.

4. Discussion: The Gulf Stream System Flow Field

Focusing now on Figures 6, 10, and 11, they represent our best estimates from mass/salt/O_2 conservation, the geostrophic assumption, and the acoustic velocity measurements of the absolute horizontal field of flow during 3.5 days in June 1982. The horizontal velocity sections for the rank 25 and 30 solu-

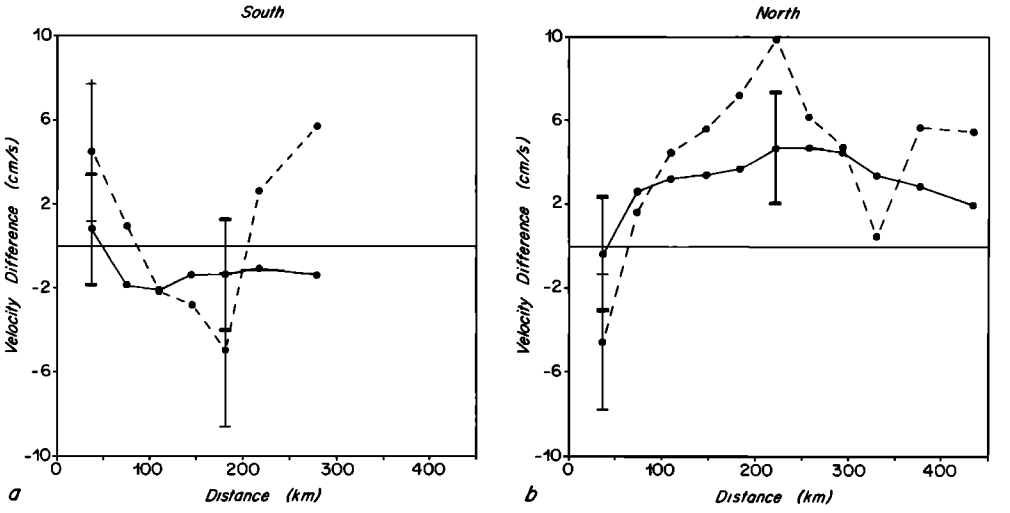

Fig. 8. Velocity differences at 2000 m between rank 25 and 30 combined inversions and that inferred from acoustic velocity plus thermal wind alone. Some typical error bars are shown. At rank 25 (dashed curve) these error bars combine the errors that are due to data noise with those from the failure to have sufficient information. At rank 30 (solid curve) the system is formally fully determined, and the errors are wholly due to noise.

tions are nearly indistinguishable by eye. The numerical transport values quoted here and plotted in Figures 10 and 11 are taken to lie between the results of these two solutions, which represent the degree of our uncertainty. A compromise estimate at rank 28 gives a horizontal velocity picture slightly closer to the rank 30 solution. No claim is made that the transports represent time-averaged conditions, and indeed we emphasize the time variability known to occur in this area. Nonetheless, in this "snapshot," one can see aspects of the flow field relatable to conventional beliefs about the large-scale time-averaged circulation of this region. *Halkin and Rossby* [1985] made a number of repeated "Pegasus" sections seaward from Chesapeake Bay over a 2.5-year period. They calculated the volume transport of the Gulf Stream relative to 2000 dbar and found a 10-Sv change in Gulf Stream transport in one week. In light of this, how certain can we be that total transport or transport in the various layers should be in balance when comparing two sections taken over a 3.5-day period? Should less weight be put on balancing layer transports and more on the acoustics? These uncertainties are reflected in our inability to choose between the rank 25 and rank 30 solutions.

Another practical matter is the definition of what we mean by the Gulf Stream. Is it all northeastward flow across each of the sections, or should it be defined on the basis of total volume transport, thus containing the DWBC counter flow in its definition in the region where the two boundary currents "cross over" each other? Also, from our velocity sections one can see that neither the south nor the north section went far enough into the Sargasso Sea to observe the decrease in northeastward flow in the upper ocean: thus in one sense, neither section crossed the entire Gulf Stream. With these caveats which may undermine the remaining confidence in the significance of anyone's transport estimates, we will calculate the net values using the entire south section and the southernmost five station pairs in the north section and briefly compare them to some of the earlier ones. From the transports in Figure 10, the total volume transport of the stream can be estimated to be 95 Sv and 119 Sv across the south and north sections, respectively, at rank 30 and 119 and 131 Sv, respectively, at rank 25. The downstream increase of the transport between our sections is about 18 Sv, which lies between estimates by *Knauss* [1969] and Halkin and Rossby east of Chesapeake Bay. It is principally the slope water transport to

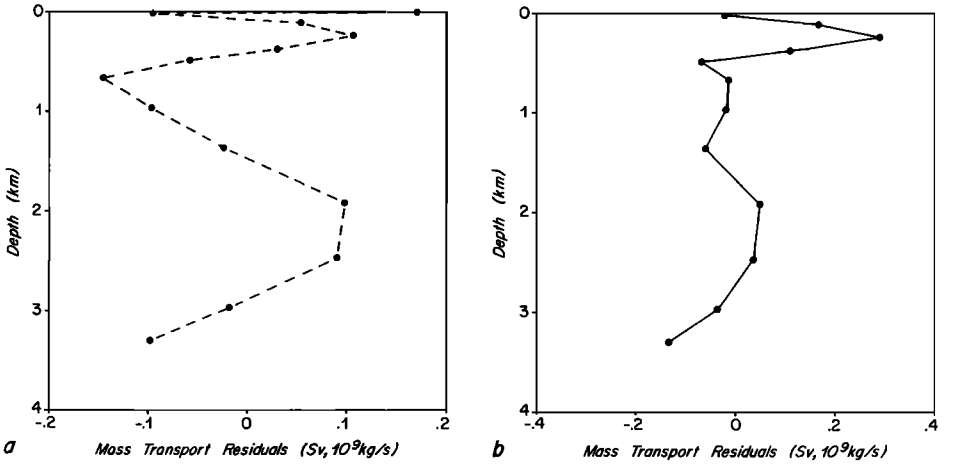

Fig. 9. Mass transport residuals as a function of layer depth in (*a*) rank 25 and (*b*) rank 30 solutions.

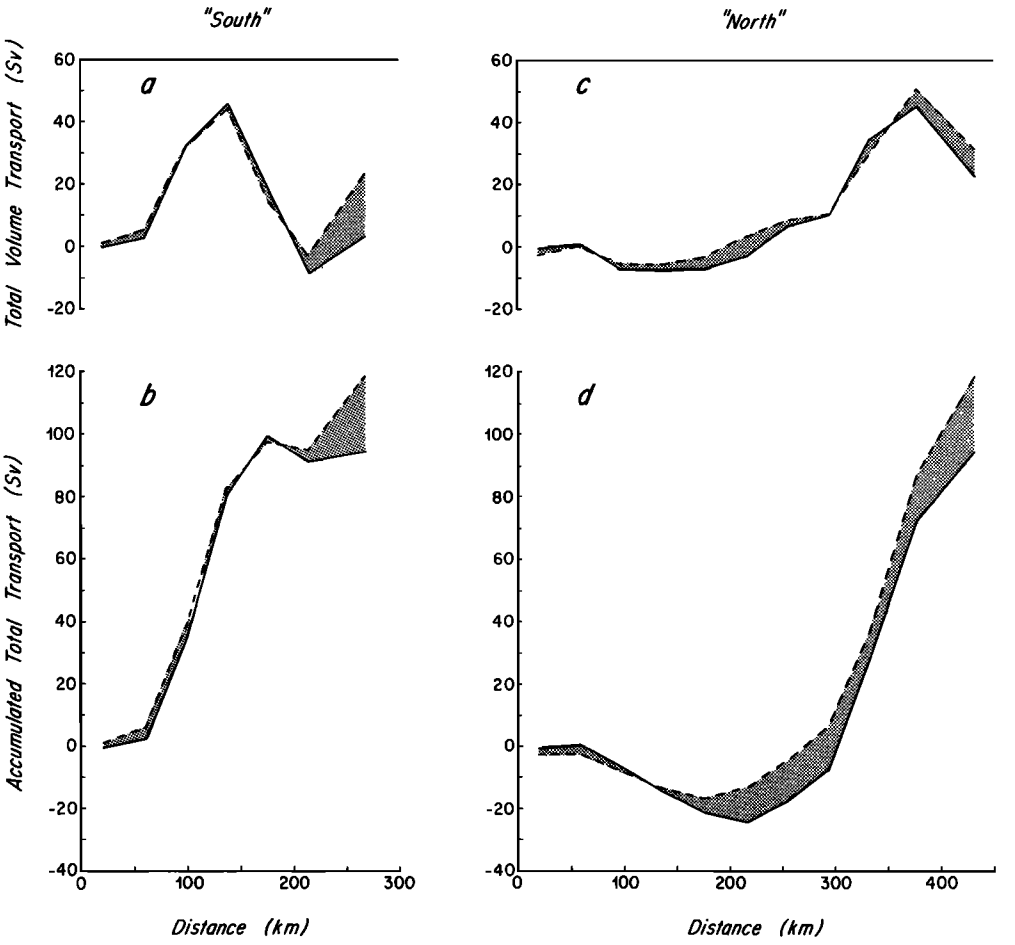

Fig. 10. Total transport (Figures 10*a* and 10*c*) and integrated transport (Figures 10*b* and 10*d*) as a function of station position for south section (Figures 10*a* and 10*b*) and north section (Figures 10*c* and 10*d*) rank 25 (dashed curves) and 30 (solid curves) combined inversions.

the southwest that accounts for the increase we observe in Gulf Stream transport immediately downstream from Cape Hatteras. We also report transport totals for the potential density layers $\sigma_\theta \leq 27.8$ (layers 1–9) and for $\sigma_\theta \geq 27.85$ (layers 11–13). Figure 12 displays the transports in schematic fashion.

The mean depth of the 27.8 potential density surface is about 2000 dbar. *Worthington* [1976, Table 10] tabulates the transport relative to this depth from a large number of different sections made over many years. The average of all the values in his table for those sections near our present south one, is 78 ± 7 Sv. Two thousand decibars is also the lower limit of integration quoted by Halkin and Rossby, who estimate the transport above that level as 88 ± 17 Sv. On the basis of the combined rank 25 and 30 solutions, we estimate a

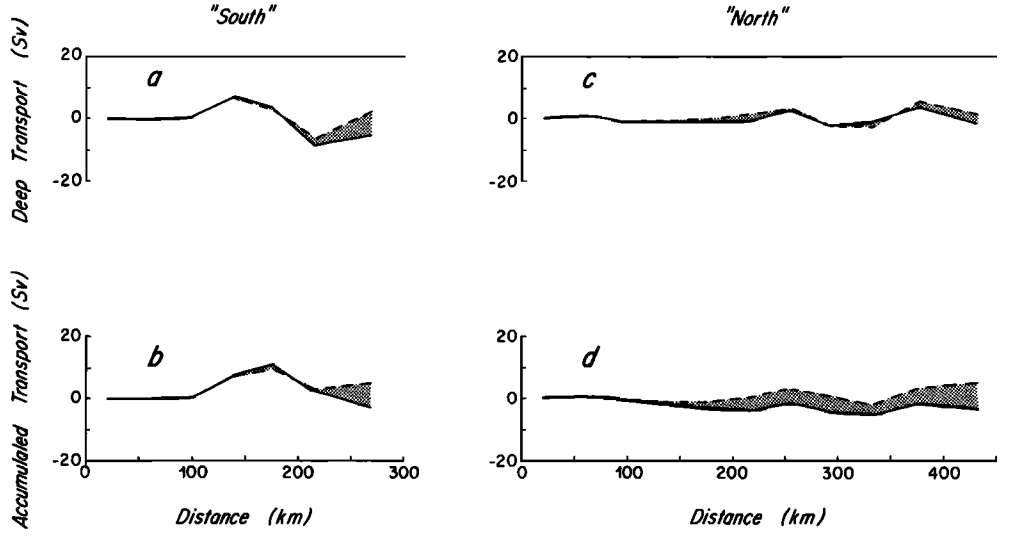

Fig. 11. Combined layer 11–13 transports as a function of station position.

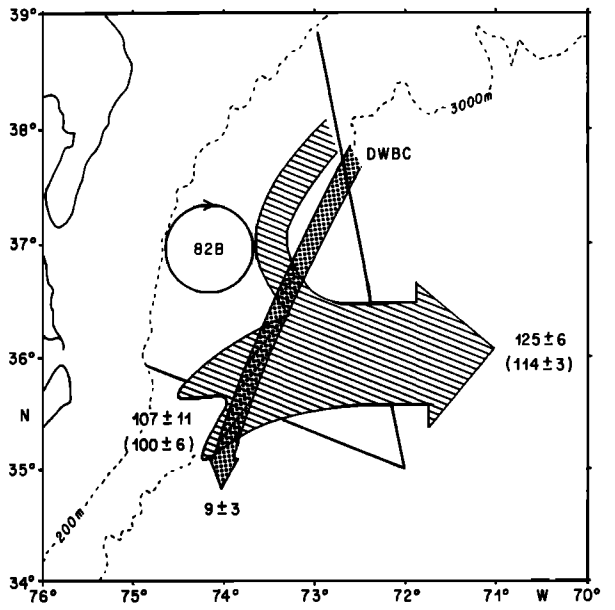

Fig. 12. Schematic summary of transport calculations from the June 1982 observations for the Gulf Stream and the deep western boundary current. Two sets of figures are given for the Gulf Stream; the first are for the total transport, while those in parentheses are for layers 1–9. Error bars represent differences in our rank 25 and 30 results.

Gulf Stream transport on the south section of 107 ± 11 Sv (100 ± 6 Sv above 2000 dbar). This "synoptic" estimate is somewhat larger than the result for Worthington's "mean" transport estimate but is consistent within error bars with the direct measurement.

The transport of the DWBC in the southern section can be estimated by integrating transports in layers 11–13, or from 27.85 to the bottom (Figure 11). These deep layers contain dense water with high dissolved oxygen. The southwestward volume transport of the DWBC is approximately the same in each section and is equal to 12 Sv in the rank 30 solution and 6 Sv in the rank 25 solution, or, formally, 9 ± 3 Sv. Note that these figures are the totals from all the southwestward moving water, not the section totals of Table 1. References to DWBC transport off North Carolina in the literature range from 2.6 [*Worthington*, 1976] to 24 Sv [*Richardson*, 1977]. The relative reliability of these and other estimates is uncertain both because of time changes and because of varying techniques. Our estimates are close to those of *Richardson and Knauss* [1971], who combined hydrographic and transport float sections to obtain a DWBC transport of 12 Sv. *Hogg* [1983] used long-term moored current meter results on 70°W and calculated a volume transport of 10 Sv below 1000 m. The DWBC crosses under the Gulf Stream and continues southward towards the equator near Cape Hatteras. The crossover point must have been situated somewhere between our two sections, according to Figure 6. The formal uncertainty in our reference level velocities is about 1 cm/s. A 1-cm/s error in velocity translates into a DWBC uncertainty of about 5 Sv if distributed over 36 km horizontally and 1500 m vertically. Evidently, to produce estimates more precise than the ones quoted here will require much more data, so that stable time averages with accuracies well below 1 cm/s can be obtained.

Existing theoretical ideas shed little light on whether the magnitudes found for w^* are reasonable. Values of 8×10^{-3} cm/s at rank 30, although large by the standards of Ekman pumping velocities, are not obviously out of line in a region encompassing the shears of the Gulf Stream system and boundary mixing associated with the continental rise and slope. Similarly, we have not been able to relate the vertical structure shown in Figure 7*b* to any body of ideas on vertical transfers except in a very schematic sense. The middepth and thermocline upwelling are at least consistent with notions about the requisite global return to near surface of deep waters formed at high latitudes. The near-bottom downwelling can be interpreted as an entrainment process diluting the flows of the deep western boundary currents. The downward flow out of the surface layer could be seen as the result of Ekman pumping, although our region is in the transition between the conventionally defined subpolar and subtropical gyres and neither the sign nor the magnitude to be expected for near surface convergences is clear. Beyond these crude statements we do not think it wise to go, and we offer Figure 7 as an empirical best estimate.

5. Separate Inversions

Figures 6 and 7 represent our best estimate of the flow field, combining together measurements and plausible physical constraints. It is useful to ask how well we would have done without some of the available data or without the use of some of the constraints.

5.1. *Acoustic Data Alone*

Use of the acoustic data alone has already been discussed in section 2. Figure 4 represents the flow field from an inversion in which there are 18 velocity constraints plus the single budgeting constraint of total mass conservation. The system was weighted in such a way that the solution yields a constant correction (the bias) independent of station position. The resulting fields leave mass, salt, and oxygen imbalances in the deep layers at the 8-Sv (and equivalent) level. The demand that these imbalances should be reduced provides (among other things) the extra information in the combined inversion which further corrects the acoustics for the random error. With only the acoustic constraints there is no information available about the w_i^*, as they do not even appear in the model (constraint equations) used.

Figure 8 compares the velocity of the rank 25 and 30 combined inversion with that of the nearly pure acoustic one. There is agreement within about 2.5 cm/s rms at rank 30 because we required it. Larger differences exist between the acoustic data and the rank 25 solution, which was less constrained to match the acoustic measurements.

5.2. *Pure Hydrographic Inversion*

Previously published hydrographic inversions [e.g., *Wunsch et al.*, 1983] usually employed only the equivalent of the last 50 constraints of (4), i.e., only what might be referred to as the budgeting requirements. The restriction to this type of constraint occurred only because no further information was available, not because inverse methods are restricted to such simple models (we have already shown the inversion of the combined system of equations (4)). A general rule of oceanic model making is that one should use everything one knows, leading as was discussed elsewhere to "eclectic" models. Nonetheless, it will often be true, certainly for almost all use of historical data, that no further information beyond the budgeting requirements will be available, and thus it is interesting to see how well the budgeting constraints alone can

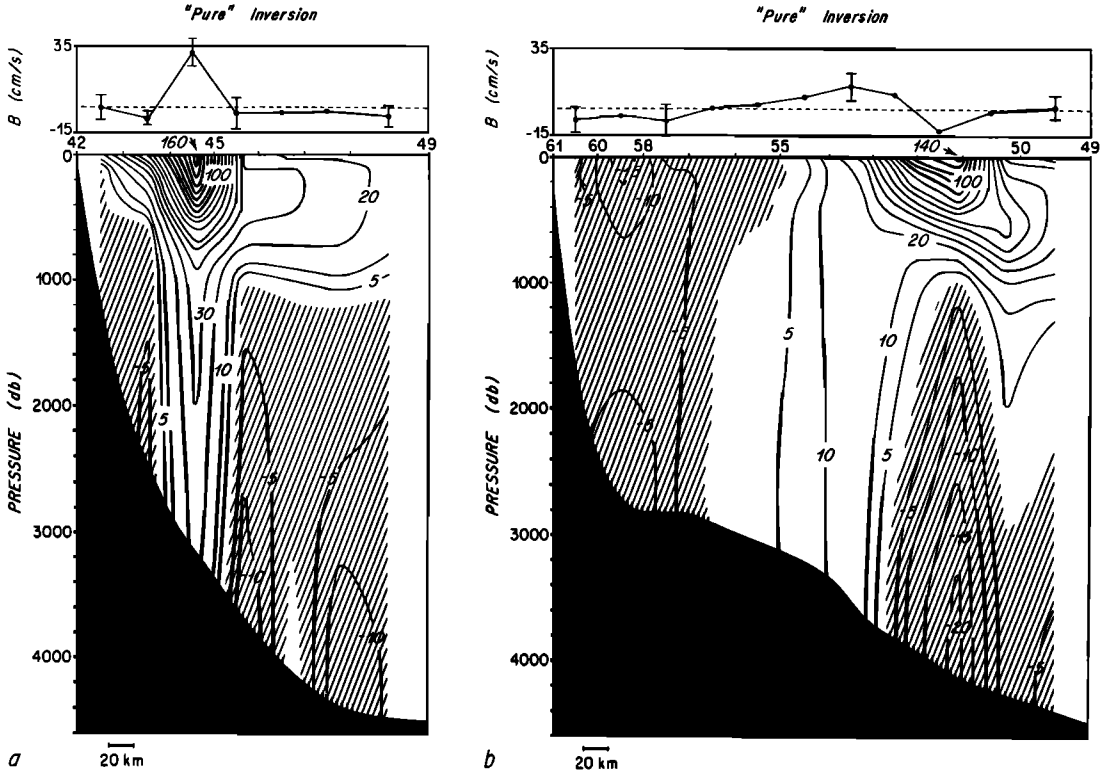

Fig. 13. Velocity sections from an inversion at rank 12, in which none of the acoustic velocity data were used (compare with Figure 6). Reference level velocity at 2000 dbar is shown at top with representative error bars; these errors are dominated by the failure to resolve and not by system noise.

do in determining the flow field. Doing this calculation means repeating the inversion, but employing only the last 50 equations of (3). The usual procedures suggested that the rank was about 12; i.e., we thus have only about 12 independent pieces of information about the 30 unknowns.

As would normally be true with hydrographic data alone, the a priori variance for $\mathbf{b}$ was taken as (a small) constant:

$$\langle b_i^2 \rangle = (10 \text{ cm/s})^2$$

with that for w_i^* the same as before. The chief effect of thus taking an a priori variance that is too small is to underestimate the resolution error for the b_i.

The rank 12 solution is displayed in Figure 13 along with the error bars. It will be seen that there is qualitative agreement in the sections between the hydrographic inversion and the independent estimate from using the acoustic data. The Gulf Stream reaches the bottom on the southern section, but there is a westward-going component present underneath in the northern one. We can make a detailed comparison, layer by layer, of the mass fluxes in the different layers for the sections of Figures 4, 6, and 13; the values are displayed in Table 1.

The resolution of the b_i (diagonal element of the resolution matrix) ranges from about 0.9 (in the second station pair of the south section) to a low of about 0.2 (in the station pairs shoreward of the Gulf Stream in the north section). For the most part, the dominant error in the b_j arises from the failure to resolve rather than from the data noise. The resolution of the w_i^* ranges from a maximum of about 0.6 just below the surface layers to a minimum near zero in the deepest isopycnal interface. Again, most of the error derives from the lack of information rather than from the noise field.

The acoustic solution is closer to the combined, best estimate solution than is the purely hydrographic inversion. This result is no surprise, as we demanded that the acoustic values be reproduced to within 3 cm/s. In a region where the reference level velocities were smaller than under the Gulf Stream (there approaching 30 cm/s), the contrast between the two types of solution would be much less marked. The qualitative features of the hydrographic inversion are, however, similar to the combined estimates (e.g., both yielding the "columnar" or "cellular" structures which are a familiar result of inversions). The pure hydrographic inverse corrections, b_i, tend to be largest where the upper level baroclinicity (and flow) is greatest.

6. Final Comments

The combination of CTD/O_2 data with acoustic velocity measurements leads to estimates of the absolute geostrophic flow field which are generally consistent with previous ones but which we believe have a smaller formal error than those in any prior determination. The general procedures of inverse methods are a powerful way of making the combination and should be useful in other areas as acoustic measurements become more widespread.

In the future, improvements in navigation should reduce the bias errors in the acoustic measurements, and there should also be a reduction in the random errors through other technical changes. LORAN units exist which have noise levels 3–4 times smaller than the one available on *Endeavor*. Similar improvements can be anticipated from new navigation systems such as Global Positioning System. A point of diminishing returns exists, however, when the ocean changes faster than it can be measured, rendering the aliasing error larger than the

instrumental error. In the present application that point has nearly been reached.

The results are encouraging for the future use of altimetric observations which will be similar in nature to the acoustic ones. In particular, notice that the combination of the acoustic measurements with hydrography can yield a high accuracy estimate of the geoid shape, as was discussed by *Wunsch and Gaposchkin* [1980]. Our present estimates of near-surface geostrophic flow have an rms error of about 1 cm/s.

An estimate of surface velocity v_s can be converted into an estimate of the surface slope through the geostrophic relationship

$$v_s = \frac{g}{f}\frac{\partial \zeta}{\partial x} \tag{5}$$

where ζ is the surface elevation. With a station spacing of about 40 km, a 1-cm/s error translates into a slope error in (5) of about 0.4 cm on this same scale, or 10^{-7}, an error far smaller than can be obtained gravimetrically [*Zlotnicki*, 1984]. Alternatively, our total transport error of about 10 Sv over distances of 400 km becomes a slope error of 3 cm, or 7.5 $\times 10^{-8}$ on this scale. Evidently, the large-scale combination of acoustic measurements with hydrography/chemistry, as has been done here, could ultimately lead to global scale geoid slope estimates if adequate altimetry is also available.

We have learned that the acoustic measurements carry information independent of the budgeting constraints (no surprise) and that the budgeting constraints carry information independent of the acoustics (also no surprise), are useful in improving acoustic measurements, and will likely show even more dramatic effects in regions of weaker currents.

Acknowledgments. This study was supported by National Science Foundation grants OCE 8501176 at Woods Hole Oceanographic Institution and OCE 8018515 at Massachusetts Institute of Technology and by National Aeronautical Space Administration grant NAG 5-534. We are grateful to Barbara Grant for the inverse calculations; to the WHOI CTD group, Jane Dunworth, and Cleo Zani for collecting and processing data; and to Lorraine Barbour, who prepared the figures.

REFERENCES

Beardsley, R. C., and W. C. Boicourt, On estuarine and continental-shelf circulation in the Middle Atlantic Bight, in *Evolution of Physical Oceanography, Scientific Surveys in Honor of Henry Stommel*, edited by B. A. Warren and C. Wunsch, pp. 198–233, MIT Press, Cambridge, Mass., 1981.

Halkin, D., and T. Rossby, The structure and transport of the Gulf Stream at 73°W, *J. Phys. Oceanogr.*, *15*, 1439–1452, 1985.

Hogg, N. G., A note on the deep circulation of the western North Atlantic: Its nature and causes, *Deep Sea Res.*, *30*, 945–961, 1983.

Joyce, T. M., D. S. Bitterman, Jr., and K. Prada, Shipboard acoustic profiling of upper ocean currents, *Deep Sea Res.*, *29*, 903–913, 1982.

Knauss, J. A., A note on the transport of the Gulf Stream, *Deep Sea Res.*, *16*, suppl., 117–123, 1969.

Lawson, C. L., and R. J. Hanson, *Solving Least Square Problems*, 340 pp., Prentice-Hall, Englewood Cliffs, N. J., 1974.

Olson, D. B., R. W. Schmitt, M. A. Kennelly, and T. M. Joyce, A two-layer diagnostic model of the long-term physical evolution of warm-core ring 82B, *J. Geophys. Res.*, *90*, 8813–8822, 1985.

Pollard, R. T., Mesoscale (50–100 km) circulations revealed by inverse and classical analysis of the JASIN hydrographic data, *J. Phys. Oceanogr.*, *13*, 377–394, 1983.

Richardson, P. L., On the crossover between the Gulf Stream and the western boundary undercurrent, *Deep Sea Res.*, *24*, 139–159, 1977.

Richardson, P. L., and J. A. Knauss, Gulf Stream and western boundary undercurrent observations at Cape Hatteras, *Deep Sea Res.*, *18*, 1089–1109, 1971.

Roemmich, D., and C. Wunsch, On combining satellite altimetry with hydrographic data, *J. Mar. Res.*, *40*, suppl., 605–618, 1982.

Volkmann, G., Deep current observations in the western North Atlantic, *Deep Sea Res.*, *9*, 493–500, 1962.

Webster, F., Vertical profiles of horizontal ocean currents, *Deep-Sea Res.*, *16*, 85–98, 1969.

Worthington, L. V., *On the North Atlantic Circulation*, 110 pp., Johns Hopkins Press, Baltimore, Md., 1976.

Worthington, L. V., and H. Kawai, Comparison between deep sections across the Kuroshio and the Florida Current and Gulf Stream, in *Kuroshio, Its Physical Aspects*, edited by H. Stommel and K. Yoshida, pp. 371–385, University of Tokyo Press, Tokyo, 1972.

Wunsch, C., The general circulation of the North Atlantic west of 50°W determined from inverse methods, *Rev. Geophys.*, *16*, 583–620, 1978.

Wunsch, C., Can a tracer field be inverted for velocity?, *J. Phys. Oceanogr.*, *11*, 1521–1531, 1985.

Wunsch, C., and E. M. Gaposchkin, On using satellite altimetry to determine the general circulation of the oceans with application to geoid improvement, *Rev. Geophys.*, *18*, 725–745, 1980.

Wunsch, C., D. Hu, and B. Grant, Mass, heat, salt, and nutrient fluxes in the South Pacific Ocean, *J. Phys. Oceanogr.*, *13*, 725–753, 1983.

Zlotnicki, V., On the accuracy of gravimetric geoids and the recovery of oceanographic signals from altimetry, *Mar. Geod.*, *8*, 129–157, 1984.

T. M. Joyce, Woods Hole Oceanographic Institution, Woods Hole, MA 02543.

S. D. Pierce, Joint Program in Oceanography, Massachusetts Institute of Technology/Woods Hole Oceanographic Institution, Woods Hole, MA 02543.

C. Wunsch, Department of Earth, Atmospheric, and Planetary Sciences, Massachusetts Institute of Technology, Cambridge, MA 02139.

(Received November 15, 1985;
accepted January 28, 1986.)